Peer-reviewed version available at Entropy 2017, 19, 168; doi:10.3390/e19070168

Article

On Unsteady Three-Dimensional Axisymmetric MHD Nanofluid Flow with Entropy Generation and Thermo-Diffusion Effects

Mohammed Almakki [1], Sharadia Dey [1]*, Sabyasachi Mondal[1] and Precious Sibabda [1]

[1] School of Mathematics, Statistics and Computer Science, University of KwaZulu-Natal, Pietermaritzburg Private Bag X01, Scottsville 3209, South Africa

* Correspondence: sharadiadey1985@gmail.com

Academic Editor: name
Received: date; Accepted: date; Published: date

Abstract: We investigate entropy generation in unsteady three-dimensional axisymmetric MHD nanofluid flow over a non-linearly stretching sheet. The flow is subject to thermal radiation and a chemical reaction. The conservation equations were solved using the spectral quasi-linearization method. The novelty of the work is in the study of entropy generation in three-dimensional axisymmetric MHD nanofluid and the choice of the spectral quasilinearization method as the solution method. The effects of Brownian motion and thermophoresis are also taken into account when the nanofluid particle volume fraction on the boundary in passively controlled. The results show that as the Hartman number increases, both the Nusselt number and the Sherwood number decrease whereas the skin friction increases. It is further shown that an increase in the thermal radiation parameter corresponds to a decrease in the Nusselt number. Moreover, entropy generation increases with the physical parameters.

Keywords: Unsteady 3-D axisymmetric nanofluid; Entropy generation; Spectral quasi-linearization method.

1. Introduction

The study of unsteady nanofluid flow, heat and mass transfer from a nonlinear stretching surface has received considerable attention during the last few years because of several applications in engineering processes, for instance, in materials manufacturing through extrusion, glass-fiber and paper production. Similarly, unsteady mixed convection in boundary layer flows has received attention with a large number of studies focusing on heat and mass transfer characteristics in nanofluids, Dessie et al. [1]. Nanofluids have been shown to have increased thermal conductivity and convective heat transfer performance compared to base fluids such as water and oils. The notion of a nanofluid was introduced by Choi[2] when he proposed the suspension of nanoparticles in a base fluid like water, oil and ethylene-glycol mixture. These common base fluids have lower thermal conductivity which is increased when nanoparticles are added. The increase in the thermal conductivity was explained by Buongiorno [3] in terms of the effect of particle Brownian motion and thermophoresis. Nanofluids have many applications due to the unique chemical and physical properties of the constituent nanoparticles. For instance, nanofluids have been used in applications that require high-performance cooling systems such as hot rolling, glass fibre production, rubber and the manufacture of metallic sheets [4].

Heat transfer due to free and mixed convection has many applications in, for example, electronic cooling, heat exchangers etc. The study of axisymmetric MHD flow and heat transfer of power law fluid along an unsteady radially stretching sheet was carried out by Ahmed et al.[5]. The conservation equations were solved analytically and numerically. The study showed that the thermal boundary layer thickness decreased with the Prandtl number and the unsteadiness parameter. Mohammadiun et al.[6] derived an exact solution of axisymmetric stagnation-point flow and heat transfer along a

Peer-reviewed version available at Entropy 2017, 19, 168; doi:10.3390/e19070168

stationary infinite circular cylinder of a steady viscous compressible fluid with constant heat flux. The general self-similar solution was obtained with constant wall heat flux. The solutions of the system were obtained for different Reynolds numbers, compressibility factors and Prandtl numbers.

Shankar et al. [7] studied heat and mass transfer in MHD boundary-layer flow of a nanofluid along a stretching boundary with a non uniform heat source/sink. The system of equations were solved numerically using the Keller-box method. The study of MHD effects in heat transfer has been a subject of research due to its potential applications in many branches of science and technology. In MHD flow the induced currents in the fluid generate forces which, in turn, modify the flow field. Shahzad et al.[8], provided the exact solution for the MHD flow and heat transfer from a viscous incompressible fluid and a nonlinear radially stretching sheet in a porous medium.

Thermal radiation is important in the flow of a fluid and consequently the effects of thermal radiation on heat and mass transfer have been extensively studied. Ahmad et al.[9] considered the effect of thermal radiation on steady MHD axisymmetric stagnation point flow of a viscous incompressible micropolar fluid along a shrinking sheet. The system of equations were solved numerically using an algorithm based on finite difference approximations. They found that the thickness of the thermal boundary layer become thinner as the thermal radiation parameter increased. The effect of melting heat transfer and second order slip in presence of the thermal radiation on stagnation point flow was examined by Mabood et al. [10]. Singh et al. [11] analyzed unsteady MHD flow of a viscous incompressible fluid over a permeable stretching sheet and took into account the effect of thermal radiation.

In many practical applications mass transfer takes place by molecular diffusion of species in homogeneous and heterogeneous chemical reactions, Sarada et al.[12]. The diffusive species can be generated or absorbed in the fluid which can affect the properties and quality of finished products. For this reasons a chemical reaction is of great practical importance to engineers and scientists. Sarada et al. [12] analyzed the influence of a chemical reaction on unsteady MHD flow of a viscous incompressible fluid past an infinite vertical porous plate with variable suction.

The study of the unsteady flow of a viscous incompressible fluid along a linear stretching with a chemical reaction was investigated by Hunegnaw et al. [13]. They used a shooting technique and a fourth-order Runge-Kutta integration scheme combined with Newton Raphson method to solve the conservation equations. Barik [14] presented a study on the effects of a chemical reaction on unsteady rotating MHD flow in a porous medium with a heat source.

An important factor to consider in heat transfer processes is that of entropy generation. Entropy is a measure of the randomness or molecular disorder of a system. In accordance with the second law of thermodynamics, the entropy of a system always increases during an irreversible process and remains constant during a reversible process, that is, entropy generation (E_{gen}) is always positive for an irreversible process or zero for reversible process. The performance of any engineering system is degraded by irreversibility and entropy generation is a measure of the magnitude of the irreversibility of the process.

Entropy generation is disregarded in most of the studies reviewed earlier. In the present work, the mechanisms for generating entropy are connected to heat transfer, fluid friction irreversibility, magnetic field and mass transfer. The pioneer work in the analysis of entropy generation was done by Bejan [15]. Subsequently, entropy generation in MHD Casson nanofluid flow in the proximity of a stagnation point was investigated by Qing et al.[16]. This study assumed the flow was subject to thermal radiation and a chemical reaction. The findings suggested a positive correlation between entropy generation and an increase in the Brinkman number, Reynold number, Hartman number, and porosity. Rashidi et al.[17] considered entropy generation in nanofluid flow along a permeable stretching sheet near the stagnation point with heat generation/absorption and a convective boundary condition. Entropy generation was further studied by Rashidi et al.[18] for a rotating disk submerged in a nanofluid. The study of entropy generation in nanofluids is a growing area of research and recent studies have examined different source terms and flow geometries [19].

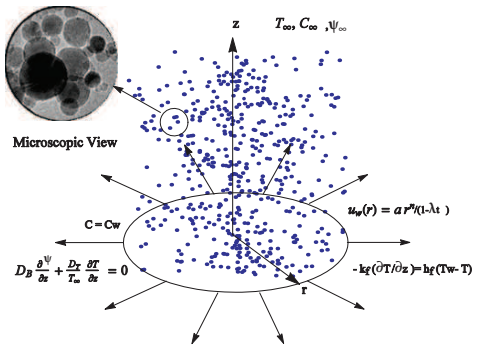

Figure 1. Physical configuration and coordinate system.

The spectral quasi-linearization method (SQLM) has not been previously used to solve equations for three-dimensional axisymmetric MHD nanofluid flow. Further, to the authors' knowledge, entropy generation in this type of fluid flow has not been previously studied. The aim of the study is to analyze thermo-diffusion effects in three-dimensional axisymmetric MHD nanofluid flow, heat and mass transfer over a nonlinearly circular stretching sheet with thermal radiation and a chemical reaction and entropy generation. The conservation equations are solved numerically using the spectral quasi-linearization method (SQLM), [20]. The SQLM combines fast convergence with accuracy. The method has been used in recent boundary layer flow and heat transfer studies such as in [20,21]. In addition, we have used the nanofluid boundary condition suggested in Nield et al.[22], namely that the nanoparticle mass flux at the wall vanishes. The results are shown to compare favourably with published work, such as Mustafa et al. [23].

2. Formulation of the problem

Consider the unsteady three-dimensional MHD flow of an incompressible viscous flow of nanofluid. A cylindrical coordinate system (r, θ, z) is used in this study. The velocity of the stretching sheet is assumed to be nonlinear along the radial direction. It is assumed that the nanoparticle mass flux at the wall is zero and the surface is stretching along the z direction, T_w, C_w and ψ_w represent the constant temperature, solutal concentration and nanoparticle concentration respectively at the wall. In the ambient fluid, the temperature, solutal concentration and nanoparticle concentration are denoted by T_∞, C_∞ and ψ_∞, respectively (see Figure 1). The variable magnetic field intensity is denoted by $B(r,t)$ where t represents time. The magnetic field acts in the positive z-direction normal to sheet. In this study, $B(r,t)$ generalizes the magnetic field term provided previously in [7,8] to

$$B(r,t) = \frac{B_0 r^{(n-1)/2}}{\sqrt{1-\lambda t}}, \tag{1}$$

where B_0 is the uniform magnetic field strength, $n > 0$ is the power-law index or stretching parameter and λ represents the unsteadiness parameter.

The equations for the conservation of mass, momentum, energy, and nanoparticle volume fraction, under the usual boundary layer assumptions can be obtained [23,24] as

$$\frac{\partial u}{\partial r}+\frac{u}{r}+\frac{\partial w}{\partial z}=0, \tag{2}$$

$$\frac{\partial u}{\partial t}+u\frac{\partial u}{\partial r}+w\frac{\partial u}{\partial z}=\nu_f\frac{\partial^2 u}{\partial z^2}-\frac{\sigma B^2(r,t)u}{\rho_f}, \tag{3}$$

$$\frac{\partial T}{\partial t}+u\frac{\partial T}{\partial r}+w\frac{\partial T}{\partial z}=\alpha_f\frac{\partial^2 T}{\partial z^2}+\tau\left[D_B\frac{\partial \psi}{\partial z}\frac{\partial T}{\partial z}+\frac{D_T}{T_\infty}\left(\frac{\partial T}{\partial z}\right)^2\right]+D_{TC}\frac{\partial^2 C}{\partial z}-\frac{1}{\rho_f c_p}\frac{\partial q_r}{\partial z}, \tag{4}$$

$$\frac{\partial C}{\partial t}+u\frac{\partial C}{\partial r}+w\frac{\partial C}{\partial z}=D_s\frac{\partial^2 C}{\partial z^2}+D_{CT}\frac{\partial^2 T}{\partial z}-R(r,t)(C-C_\infty), \tag{5}$$

$$\frac{\partial \psi}{\partial t}+u\frac{\partial \psi}{\partial r}+w\frac{\partial \psi}{\partial z}=D_B\frac{\partial^2 \psi}{\partial z^2}+\frac{D_T}{T_\infty}\frac{\partial^2 T}{\partial z^2}, \tag{6}$$

where u and w represent the fluid velocity components in r and z directions respectively; ν_f, σ and ρ_f are the kinematic viscosity, electrical conductivity and the viscosity of the fluid, respectively; $\alpha_f = k_f/(\rho c_p)_f$ is the thermal diffusivity, c_p is the heat capacity, D_B is the Brownian diffusion coefficient, D_T is the thermophoretic diffusion coefficient; $\tau = (\rho c_p)_s/(\rho c_p)_f$ the ratio of effective heat capacity of the nanoparticle material to heat capacity of the fluid; D_{CT} and D_{TC} are the Soret and Dufour diffusivities, D_s is the solutal diffusivity and $R(r,t)$ is the chemical reaction.

The quantity q_r represents the relative heat flux. Applying the Rosseland approximation [25], q_r can be expressed as

$$q_r=-\frac{4\sigma^*}{3K^*}\frac{\partial T^4}{\partial z}, \tag{7}$$

where σ^* is the Stephen- Boltzmann constant and K^* the Rosseland mean spectral absorption coefficient. If the temperature differences across the flow are small, such that T^4 maybe expanded using Taylor series about T_∞, then

$$T^4 \approxeq 4T_\infty^3 T-3T_\infty^4. \tag{8}$$

Substituting Equation (8) in Equation (7), the relative heat flux becomes

$$q_r=-\frac{16\sigma^* T_\infty^3}{3K^*}\frac{\partial T}{\partial z}. \tag{9}$$

To reduce the complexity of the mass equation, the chemical reaction $R(r,t)$ must be a constant. This condition holds if $R(r,t)$ has the following form

$$R(r,t)=R_0\frac{ar^{n-1}}{1-\lambda t}, \tag{10}$$

where R_0 is constant and $a > 0$ is the stretching constant.

The boundary conditions considered in this work (see [23]) are

$$
\begin{aligned}
u = u_w(r) = \frac{ar^n}{1-\lambda t},\ -k_f\frac{\partial T}{\partial z} = h_f(T_w - T),\\
D_B\frac{\partial \psi}{\partial z} + \frac{D_T}{T_\infty}\frac{\partial T}{\partial z} = 0,\ C = C_w \ \text{ at } z = 0,\\
u \to 0,\ T \to T_\infty,\ C \to C_\infty \text{ and}\\
\psi \to \psi_\infty \text{ as } z \to \infty,
\end{aligned} \tag{11}
$$

where $k_f = k_0\sqrt{1-\lambda t}$ is the thermal conductivity of the base fluid where k_0 is a constant. A similarity solution of the energy equation can be obtained if the Biot number,

$$
Bi = \frac{h_f}{k_0}\sqrt{\frac{\nu_f}{ar^{(n-1)}}}, \tag{12}
$$

is a constant. This condition is satisfied if the heat transfer coefficient, h_f, is proportional to $r^{(n-1)/2}$. Thus, the heat transfer coefficient is expressed as $h_f = b_0 r^{(n-1)/2}$, where b_0 is a constant. The Biot number can be written as $Bi = h_0\sqrt{(\nu_f/a)}/k_0$.

Equations (2)-(6) are transformed into ordinary differential equations by using the following similarity variables (see[23])

$$
\begin{aligned}
\eta = \sqrt{\frac{a}{\nu_f(1-\lambda t)}}r^{(n-1)/2}z,\ \theta(\eta) = \frac{T - T_\infty}{T_w - T_\infty},\\
S(\eta) = \frac{C - C_\infty}{C_w - C_\infty},\ \phi(\eta) = \frac{\psi - \psi_\infty}{\psi_\infty}.
\end{aligned} \tag{13}
$$

The system of Equations (2)−(6) are transformed to

$$
f''' + \frac{(n+3)}{2}ff'' - nf'^2 - A\left(f' + \frac{1}{2}\eta f''\right) - Haf' = 0, \tag{14}
$$

$$
\left(1 + Nr\right)\frac{1}{Pr}\theta'' - \frac{A}{2}\eta\theta' + \frac{n+3}{2}f\theta' + Nb\phi'\theta' + Nt\theta'^2 + Nd\,S'' = 0, \tag{15}
$$

$$
\frac{1}{Sc}S'' - \frac{A}{2}\eta S' + \frac{(n+3)}{2}fS' - R_0S + Ld\,\theta'' = 0, \tag{16}
$$

$$
\phi'' - \frac{A}{2}Sc\,\eta\phi' + \frac{n+3}{2}Sc\,f\phi' + \frac{Nt}{Nb}\theta'' = 0, \tag{17}
$$

subject to the boundary conditions

$$
\begin{aligned}
f(0) = 0,\ \ f'(0) = 1 \text{ and } f'(\infty) \to 0,\\
\theta'(0) = -Bi(1 - \theta(0)),\ \theta(\infty) \to 0,\\
S(0) = 1,\ S(\infty) \to 0,\\
Nb\phi'(0) + Nt\theta'(0) = 0 \text{ and } \phi(\infty) \to 0.
\end{aligned} \tag{18}
$$

The parameters in Equations (14)-(17) are given by

$$A = \frac{\lambda}{ar^{n-1}},\ Ha = \frac{\sigma B_0^2}{a\rho_f},\ Pr = \frac{\nu_f}{\alpha},\ Nr = \frac{16\sigma^* T_\infty^3}{3k_f K^*},$$
$$Nb = \frac{\tau D_B \phi_\infty}{\nu_f}, Nt = \frac{\tau(T_w - T_\infty)D_T}{\nu_f T_\infty},$$
$$Nd = \frac{D_{TC}(C_w - C_\infty)}{\nu_f(T_w - T_\infty)},\ Sc = \frac{\nu_f}{D_B},$$
$$R_0 = \frac{(1-\lambda t)R(x,t)}{ar^{n-1}} \text{ and } Ld = \frac{D_{CT}(T_w - T_\infty)}{\nu_f(C_w - C_\infty)}, \tag{19}$$

where A is the unsteadiness parameter, Ha is the Hartman number, Pr is the Prandtl number, Nr is the thermal radiation parameter, Nb is the Brownian motion parameter, Nt is the thermophoresis parameter, Nd is the modified Dufour parameter, Sc is the Schmidt number, R_0 is a constant and Ld is the modified Soret parameter.

The skin friction coefficient C_f, the Nusselt number Nu_r and the Sherwood number Sh_r can be expressed as

(i) Skin-fraction coefficient:

$$C_f Re^{1/2} = f''(0), \tag{20}$$

where $Re = \frac{u_w(r)r}{\nu_f}$ is Reynolds number.

(ii) Nusselt number:

$$Nu = \frac{rh_w}{k_f(T_w - T_\infty)}, \tag{21}$$

where h_w represents surface heat flux, which can obtain by

$$h_w = -\left[k_f + \frac{16\sigma^* T_\infty^3}{3K^*}\right]\left(\frac{\partial T}{\partial z}\right)_{z=0}. \tag{22}$$

Equation (21) becomes as

$$-(1+Nr)\theta'(0) = Re^{-1/2}Nu \tag{23}$$

(iii) The Sherwood number for solutal concentration equation is

$$Sh_r = \frac{rh_m}{D_s(C_w - C_\infty)}, \tag{24}$$

where

$$h_m = -D_s\left(\frac{\partial C}{\partial z}\right)_{z=0}, \tag{25}$$

where h_m is the surface mass flux. Equation (24) can be written as

$$-\varphi'(0) = Re_r^{-(1/2)} Sh_r \tag{26}$$

The mass flux is zero due to the nanoparticle boundary condition used, and for this reason, it is not possible to define the Sherwood number for nanoparticle concentration at the wall.

3. Entropy generation analysis

Entropy generation is associated with a wastage of energy, hence minimization of entropy production is a key design objective. Entropy generation analysis can be used as an effective tool for identification of the causes of inefficiency in any system and offers scope for the improvement in design of any device/ process. This analysis provides an insight into the efficiency of usage of thermal energy in different industrial processes, and may, in principle be used for any type of energy conservation system.

The limitation of global energy resources has driven the scientific community to reexamine energy production systems, conversion and consumption, Arikoglu et. al [26]. From a theoretical perspective, the second law of thermodynamics is utilized to study energy producing, converting and consuming systems. The volumetric rate of local entropy generation for a nanofluid, with thermal radiation and a magnetic field, can be expressed as (see [16,18,19];

$$E_{gen} = \underbrace{\frac{k}{\widetilde{T}_\infty^2}\left(\left(\frac{\partial \widetilde{T}}{\partial z}\right)^2 + \frac{16\sigma^* \widetilde{T}_\infty^3}{3K^*}\left(\frac{\partial \widetilde{T}}{\partial z}\right)^2\right)}_{1^{st}\text{ part}} + \underbrace{\frac{\mu}{\widetilde{T}_\infty}\left(\frac{\partial \widetilde{u}}{\partial z}\right)^2}_{2^{nd}\text{ part}} + \underbrace{\frac{\sigma B_0^2}{\widetilde{T}_\infty}\widetilde{u}^2}_{3^{rd}\text{ part}} + \underbrace{\frac{RD_B}{\psi_\infty}\left(\frac{\partial \psi}{\partial z}\right)^2 + \frac{RD_B}{\widetilde{T}_\infty}\left(\frac{\partial T}{\partial z}\right)\left(\frac{\partial \psi}{\partial z}\right)}_{4^{th}\text{ part}} \tag{27}$$

In Equation (27), the entropy generation is stated in four parts. The first part is entropy generation due to heat transfer irreversibility; the second part is the entropy generation due to the viscous dissipation irreversibility; the third part is the entropy generation due to the applied magnetic field irreversibility and the fourth part is due to the diffusive irreversibility.

We define the entropy generation number as the ratio of the local volumetric entropy generation rate E_{gen} to a characteristic rate of entropy generation E_0, that is,

$$N_G = \frac{E_{gen}}{E_0}, \tag{28}$$

where

$$E_0 = \frac{k_f (T_w - T_\infty)^2}{T_\infty^2 r^2}. \tag{29}$$

Using Equations (27)-(29), the non-dimensionless entropy generation can be written as

$$N_G = Re(1+Nr)\theta'^2(\eta) + \frac{BrRe}{\Omega} f''^2 + \frac{Br(Ha)^2}{\Omega} f'^2 + \frac{Re\Sigma}{\Omega^2}\phi'^2(\eta) + \frac{Re\Sigma}{\Omega}\theta'(\eta)\phi'(\eta), \tag{30}$$

where $Re, Nr, Br, \Omega, Ha, \Sigma$ are Reynolds number, thermal radiation parameter, Brinkman number, dimensionless temperature difference, Hartman number and diffusive constant parameter,

respectively. Some of these parameters are defined before. These numbers are expressed by the following relations

$$Br = \frac{\mu u_w^2}{k_f \Delta T}, \Omega = \frac{\Delta T}{T_\infty} = \frac{T_w - T_\infty}{T_\infty}, \Sigma = \frac{R D_B \psi_\infty}{k_f}. \tag{31}$$

4. Method of solution

The quasilinearization method (QLM) is a generalization of the Newton-Raphson method, see Bellman and Kalaba [27]. The derivation of the QLM is based on the linearization of the nonlinear components of the governing equations using the Taylor series assuming that the difference between the value of the unknown function is negligible between the current iteration (denoted by $r+1$) and the previous one (denoted by r). Applying the quasilinearization scheme to Equations (14)-(17), yields the following iterative scheme

$$a_{0,r} f'''_{r+1} + a_{1,r} f''_{r+1} + a_{2,r} f'_{r+1} + a_{3,r} f_{r+1} = R_f, \tag{32}$$

$$b_{0,r} \theta''_{r+1} + b_{1,r} \theta'_{r+1} + b_{2,r} \theta_{r+1} + + b_{3,r} f_{r+1} + b_{4,r} S''_{r+1} + b_{5,r} \phi'_{r+1} = R_\theta, \tag{33}$$

$$c_{0,r} S''_{r+1} + c_{1,r} S'_{r+1} + c_{2,r} S_{r+1} + c_{3,r} f_{r+1} + c_{4,r} \theta''_{r+1} = R_S, \tag{34}$$

$$d_{0,r} \phi''_{r+1} + d_{1,r} \phi'_{r+1} + d_{2,r} f_{r+1} + d_{3,r} \theta''_{r+1} = R_\phi, \tag{35}$$

subject to

$$\begin{aligned} & f_{r+1}(0) = 0,\ f'_{r+1}(0) = 1,\ f'_{r+1}(\infty) \to 0, \\ & \theta'_{r+1}(0) = -Bi(1 - \theta_{r+1}(0)),\ \theta_{r+1}(\infty) \to 0, \\ & S_{r+1}(0) = 1,\ S_{r+1}(\infty) \to 0, \\ & Nb\phi'_{r+1}(0) + Nt\theta'_{r+1}(0) = 0, \text{ and } \phi_{r+1}(\infty) \to 0, \end{aligned} \tag{36}$$

where the coefficients in Equations(32)-(35) are obtained as

$$a_{0,r} = 1,\ a_{1,r} = \left(\frac{n+3}{2}\right) f_r - \frac{A}{2}\eta,$$
$$a_{2,r} = -2n f_r' - A - Ha,\ a_{3,r} = \left(\frac{n+3}{2}\right) f_r'', \tag{37}$$
$$b_{0,r} = \left(1 + Nr\right)\frac{1}{Pr},$$
$$b_{1,r} = \left(\frac{n+3}{2}\right) f_r - \frac{A}{2}\eta + Nb\phi_r' + 2Nt\theta_r',$$
$$b_{2,r} = 0,\ b_{3,r} = \left(\frac{n+3}{2}\right)\theta_r',$$
$$b_{4,r} = Nd,\ b_{5,r} = Nb\theta_r', \tag{38}$$
$$c_{0,r} = \frac{1}{Sc},\ c_{1,r} = \left(\frac{n+3}{2}\right) f_r - \frac{A}{2}\eta,\ c_{2,r} = -R_0,$$
$$c_{3,r} = \left(\frac{n+3}{2}\right) S_r',\ c_{4,r} = Ld, \tag{39}$$
$$d_{0,r} = 1,\ d_{1,r} = \left(\frac{n+3}{2}\right) Sc\ f_r - \frac{A}{2} Sc\ \eta,$$
$$d_{2,r} = \left(\frac{n+3}{2}\right) Sc\ \phi_r',\ d_{3,r} = \frac{Nt}{Nb}. \tag{40}$$

A Chebyshev pseudo-spectral method, [20] was used to solve Equatios.(32)-(35). The Chebyshev interpolating polynomials defined by Equation(41) are used with Gauss-Lobatto points [28,29] to define the unknown functions where

$$x_i = \cos\left(\frac{\pi i}{N}\right), \quad i = 0, 1, ..., N; \quad -1 \leq x_i \geq 1. \tag{41}$$

The variable N in Equation(41) is the number of collocation points used. A truncated domain $[0, L]$ is used to approximate the semi-infinite domain to facilitate computations. The parameter L represents the boundary condition at infinity. In order to model the behaviour of the flow at infinity, the parameter L should be a large number. The domain $[0, L]$ is transformed into $[-1, 1]$ using the linear transformation $\eta = \frac{L(x+1)}{2}$.

The spectral collocation method is used to construct a differentiation matrix to approximate the derivative of unknown variables at the collocation points as a matrix vector product

$$\frac{dF_r^{(1)}}{d\eta}(\eta_j) = \sum_{k=0}^{N} \mathbf{D}_{jk} f(\eta_k) = \mathbf{D}F_m, j = 0, 1, 2, ..., N, \tag{42}$$

where $\mathbf{D} = 2D/L$ and $F = \left[f(\eta_0), f(\eta_1), f(\eta_1), ..., f(\eta_N)\right]^T$ represent the vector function at the collocation points. The high order derivatives are given as powers of $\mathbf{D}$ such as

$$F_r^{(p)} = \mathbf{D}^p F_r, \tag{43}$$

where p is the order of the derivative. Spectral collocation is applied at r using the differentiation matrix $\mathbf{D}$ in order to approximate derivatives of unknown functions in Equations(32)-(35) which yields

Peer-reviewed version available at Entropy 2017, 19, 168; doi:10.3390/e19070168

$$\mathbf{A}_{1,1}\mathbf{f} + \mathbf{A}_{1,2}\boldsymbol{\theta} + \mathbf{A}_{1,3}\mathbf{S} + \mathbf{A}_{1,4}\boldsymbol{\phi} = R_f, \tag{44}$$
$$\mathbf{A}_{1,2}\mathbf{f} + \mathbf{A}_{2,2}\boldsymbol{\theta} + \mathbf{A}_{2,3}\mathbf{S} + \mathbf{A}_{2,4}\boldsymbol{\phi} = R_\theta, \tag{45}$$
$$\mathbf{A}_{1,3}\mathbf{f} + \mathbf{A}_{2,3}\boldsymbol{\theta} + \mathbf{A}_{3,3}\mathbf{S} + \mathbf{A}_{3,4}\boldsymbol{\phi} = R_S, \tag{46}$$
$$\mathbf{A}_{1,4}\mathbf{f} + \mathbf{A}_{2,4}\boldsymbol{\theta} + \mathbf{A}_{3,4}\mathbf{S} + \mathbf{A}_{4,4}\boldsymbol{\phi} = R_\phi. \tag{47}$$

Here

$$\begin{aligned}&\mathbf{A}_{1,1} = a_{0,r}\mathbf{D}^3 + \mathbf{diag}(a_{1,r})\mathbf{D}^2 + \mathbf{diag}(a_{2,r})\mathbf{D}\\ &+\mathbf{diag}(a_{3,r})\mathbf{I},\\ &\mathbf{A}_{1,2} = 0, \mathbf{A}_{1,3} = 0, \mathbf{A}_{1,4} = 0,\end{aligned} \tag{48}$$

$$\begin{aligned}&\mathbf{A}_{2,1} = \mathbf{diag}(b_{3,1})\mathbf{I},\\ &\mathbf{A}_{2,2} = \mathbf{diag}(b_{0,r})\mathbf{D}^2 + \mathbf{diag}(b_{1,r})\mathbf{D} + \mathbf{diag}(b_{2,r})\mathbf{I},\\ &\mathbf{A}_{2,3} = \mathbf{diag}(b_{4,r})\mathbf{D}^2, \mathbf{A}_{2,4} = \mathbf{diag}(b_{5,r})\mathbf{D},\end{aligned} \tag{49}$$

$$\begin{aligned}&\mathbf{A}_{3,1} = \mathbf{diag}(c_{3,r})\mathbf{I}, \mathbf{A}_{3,2} = \mathbf{diag}(c_{4,r})\mathbf{D}^2,\\ &\mathbf{A}_{3,3} = c_{0,r}\mathbf{D}^2 + \mathbf{diag}(c_{1,r})\mathbf{D} + (c_{2,r})\mathbf{I} \text{ and}\\ &\mathbf{A}_{3,4} = 0,\end{aligned} \tag{50}$$

$$\begin{aligned}&\mathbf{A}_{4,1} = \mathbf{diag}(d_{2,r})\mathbf{I}, \mathbf{A}_{4,2} = \mathbf{diag}(d_{3,r})\mathbf{D}^2,\\ &\mathbf{A}_{4,3} = 0, \mathbf{A}_{4,4} = \mathbf{diag}(d_{0,r})\mathbf{D} + \mathbf{diag}(d_{1,r})\mathbf{D},\end{aligned} \tag{51}$$

$$\mathbf{R}_f = \left(\frac{n+3}{2}\right)\mathbf{f_r}\mathbf{f_r''} - n\left(\mathbf{f_r'}\right)^2,\ \mathbf{R}_\phi = \left(\frac{n+3}{2}\right)Sc\ \mathbf{f_r}\boldsymbol{\phi}_\mathbf{r}', \tag{52}$$

$$\mathbf{R}_s = \left(\frac{n+3}{2}\right)\mathbf{f_r}\mathbf{S_r'} \text{ and } \mathbf{R}_\phi = \left(\frac{n+3}{2}\right)Sc\ \mathbf{f_r}\boldsymbol{\phi}_\mathbf{r}', \tag{53}$$

where **diag**() represents diagonal matrices of order $(N+1)\times(N+1)$, $\mathbf{I}$ is an $(N+1)\times(N+1)$ identity matrix and $\mathbf{f}, \boldsymbol{\theta}, \mathbf{S}$ and $\boldsymbol{\phi}$ are the values of functions f, θ, S and ϕ, respectively. Equations(44)-(47) were solved as a matrix system using the SQLM scheme where the iteration is started with initial approximate solutions obtained as

$$\begin{aligned}&f_0(\eta) = 1 - \exp(-\eta),\ \ \theta_0(\eta) = \left(\frac{Bi}{1+Bi}\right)\exp(-\eta),\\ &S_0(\eta) = \exp(-\eta) \text{ and}\\ &\phi_0(\eta) = -\left(\frac{Nt}{Nb}\right)\left(\frac{Bi}{1+Bi}\right)\exp(-\eta).\end{aligned} \tag{54}$$

The above equations can be expressed in matrix form as follows

$$\begin{bmatrix}\mathbf{A}_{11} & \mathbf{A}_{12} & \mathbf{A}_{13} & \mathbf{A}_{14}\\ \mathbf{A}_{21} & \mathbf{A}_{22} & \mathbf{A}_{23} & \mathbf{A}_{24}\\ \mathbf{A}_{31} & \mathbf{A}_{32} & \mathbf{A}_{33} & \mathbf{A}_{34}\\ \mathbf{A}_{41} & \mathbf{A}_{42} & \mathbf{A}_{43} & \mathbf{A}_{44}\end{bmatrix}\begin{bmatrix}F_{r+1}\\ \Theta_{r+1}\\ S_{r+1}\\ \Phi_{r+1}\end{bmatrix} = \begin{bmatrix}\mathbf{R}_f\\ \mathbf{R}_\theta\\ \mathbf{R}_s\\ \mathbf{R}_\phi\end{bmatrix} \tag{55}$$

Table 1. Different values of Nusselt number $-\theta'(0)$ compared with those of Mustafa et al.[23]

n	Nt	Sc	Pr	Mustafa et al. [23]	Present results
0.5	0.1	20	5	1.9112911	1.91068095
	0.5			1.2170065	1.21659065
	0.7			0.9815765	0.98122822
1.0	0.5	5	5	1.6914582	1.69104675
		10		1.4740787	1.47375172
		20		1.2861370	1.28590965
2.5	0.5	20	0.7	0.6619164	0.66986678
			5	1.4784288	1.47847763
			7	1.5758736	1.57604858

Table 2. Computed values of Skin fraction coefficient, heat transfer coefficient and mass transfer coefficient for $Nb = 0.5, Nt = 0.5, Nd = 0.02, Ld = 0.02, Sc = 7, R_0 = 0.3, Bi = 0.2,$

n	A	Ha	Nr	Pr	$f''(0)$	-$\theta'(0)$	-$S'(0)$
1					−1.43922866	−0.16417529	−2.89107257
2	0.3	0.5	0.2	7	−1.70034047	−0.16661752	−3.16939593
4					−2.12897896	−0.16969131	−3.66539915
	-0.5				−1.77701012	−0.17085800	−3.72686482
3	0	0.5	0.2	7	−1.87092985	−0.16944779	−3.54329048
	0.5				−1.96353732	−0.16749470	−3.34434681
		1.5			−2.17151786	−0.16755905	−3.37606776
3	0.3	2.5	0.2	7	−2.39114443	−0.16678981	−3.33136800
		5			−2.86708560	−0.16495200	−3.23526081
			1		−1.92657387	−0.16615306	−3.42533294
3	0.3	0.5	1.5	7	−1.92657387	−0.16464481	−3.42514164
			2		−1.92657387	−0.16310964	−3.42504767
				4	−1.92657387	−0.16585371	−3.42553409
3	0.3	0.5	0.2	5	−1.92657387	−0.16708464	−3.42554096
				9	−1.92657387	−0.16894896	−3.42668462

Table 3. The effects of the Biot number on the maximum temperature

Biot number	Maximum temperature	Change in maximum temperature %
0.1	0.1264	
0.9	0.3401	169.07
2	0.5218	53.43
5	0.7377	41.38
10	0.853	15.63
50	0.9678	13.46

5. Results and Discussion

Entropy generation in the unsteady three-dimensional MHD nanofluid flow along a non-linear stretching sheet taking into account the influence of thermal radiation and a chemical reaction was investigated. The conservation equations were solved numerically using the spectral quasilinearization method (SQLM). The SQLM has been used in a limited number of studies to solve boundary layer flow, heat and mass transfer problems (see [30]). A comparison with previously published results is shown in Table 1 when $A = 0, Ha = 0, Nr = 0, Nd = 0$ and $Ld = 0$ (i.e. in the absence of unsteadiness parameter, Hartman number, the thermal radiation number, Dufour

Preprints (www.preprints.org) | NOT PEER-REVIEWED | Posted: 17 March 2017 doi:10.20944/preprints201703.0138.v1

Peer-reviewed version available at Entropy 2017, 19, 168; doi:10.3390/e19070168

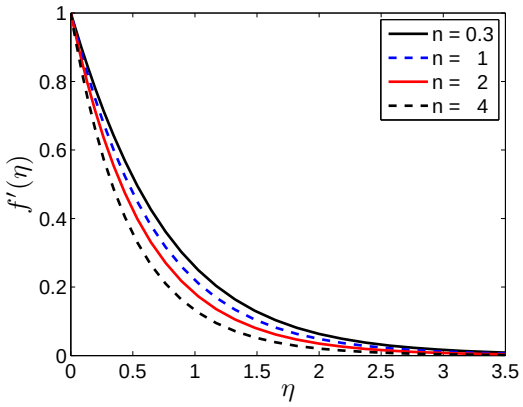

Figure 2. Effect of the stretching parameter (n) on the radial velocity profile $f'(\eta)$ when $A = 0.3, Ha = 0.5, Nr = 0.2, Pr = 7, Nb = 0.5, Nt = 0.5, Nd = 0.02, Sc = 7, R_0 = 0.3, Ld = 0.02, \beta_i = 0.2$.

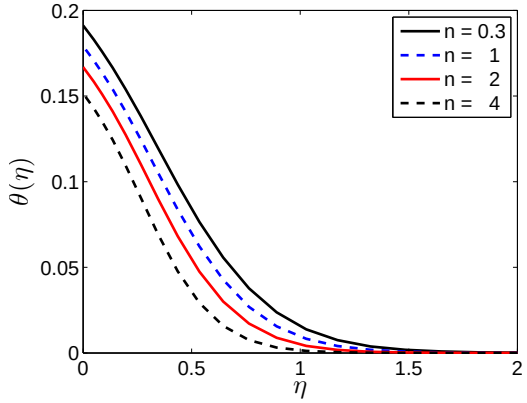

Figure 3. Effect of the stretching parameter (n) on the temperature profile $\theta(\eta)$ where $A = 0.3, Ha = 0.5, Nr = 0.2, Pr = 10, Nb = 0.5, Nt = 0.5, Nd = 0.02, Sc = 7, R_0 = 0.3, Ld = 0.02, \beta_i = 0.2$.

parameter and Soret parameter, respectively, moreover, the equation of mass is not considered). These results are comparable to those of Mustafa et al. [23] which validates this numerical method.

Below we present results that describe the impact and significance of various fluid and physical parameters on the fluid properties, the skin friction coefficient, the heat and mass transfer coefficients.

Table 2 displays the computed skin friction, heat transfer and the mass transfer coefficients which can be represented as $f''(0), |-\theta'(0)|$, and $|-S'(0)|$, respectively, for various values of n, A, Ha, Nr and Pr. It is observed that the skin friction decreases as n increases whereas the heat transfer coefficient and mass transfer increase with increasing n with other parameters fixed. It is also noted that the skin friction reduces as A increases while the heat and mass transfer rates decrease. The skin friction, heat and mass transfer rates vary inversely with Ha and appear to be independent of changes in Nr whereas the heat transfer rate decreases with Nr. The same result also holds for the skin friction and the mass transfer with respect to Pr. The heat transfer increases when Pr increases.

In Table 3 it is noted that for small values of the Biot number, small changes in the Biot number correspond to a large changes in the maximum temperature. On the contrary, for large values of the Biot number, a large change in the Biot number seems to not affect the maximum temperature significantly.

The parameter n plays an important role in fluid flow. A fluid is called pseudoplastic fluid when $n < 1$ and dilatant fluid when $n > 1$. A fluid is called a Newtonian fluid when $n = 1$. A fluid is called shear-thining or shear-thickening according as $n < 1$ or $n > 1$. The effect of n on the fluid

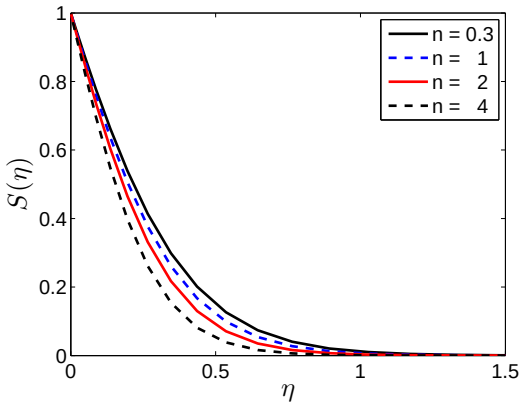

Figure 4. Effect of the stretching parameter (n) on the concentration profile $S(\eta)$ for $A = 0.3, Ha = 0.5, Nr = 0.2, Pr = 7, Nb = 0.5, Nt = 0.5, Nd = 0.02, Sc = 7, R_0 = 0.3, Ld = 0.02, \beta_i = 0.2$.

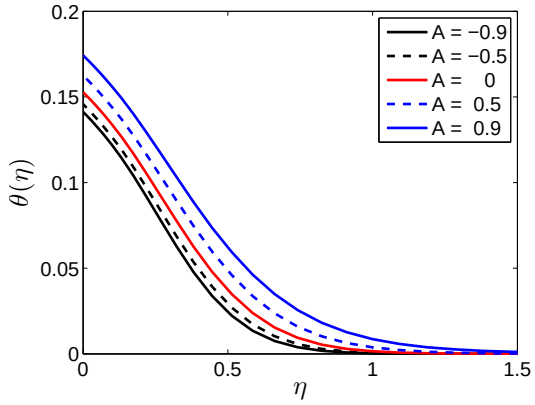

Figure 5. Effect of the unsteadiness parameter (A) on temperature profile $\theta(\eta)$ for $n = 3, Ha = 0.5, Nr = 0.2, Pr = 7, Nb = 0.5, Nt = 0.5, Nd = 0.02, Sc = 7, R_0 = 0.3, Ld = 0.02, \beta_i = 0.2$.

velocity, temperature and solutal concentration profiles, respectively are shown in Figures 2-4. Figure 2 illustrates the velocity profile (f') with the variation in the stretching sheet parameter with other parameters fixed. The magnitude of the radial component of the velocity decreases with increasing n. In contrast, n has a significant impact on η and the velocity components u and w, respectively). Figure 3 shows that an increases in n leads to a decrease in the thickness of thermal boundary layer. As a result, the temperature profiles decrease with increasing n and an increase in the heat transfer rate from the sheet. Increasing n increases the deformation rate from the wall to the fluid. Figure 4 shows the effect of n on the solutal concentration profiles when the other parameters are fixed. It is seen that increases in the non-linear stretching leads to a decrease in the solutal concentration profiles.

Figures 5 and 6 depict the effects of unsteadiness parameter A on the temperature and the solutal concentration profiles, respectively. Two cases have been studied namely $A < 0$ and $A > 0$. From Figure 5, it is observed that the temperature profiles increase with increasing values of $A > 0$. A similar effect is observed for $A < 0$. It is also observed that as the distance from the stretching sheet within the dynamic region increases, temperature decreases as unsteadiness parameter increases. Physically when unsteadiness increases the sheet looses more heat which causes a decrease in the temperature. Similar properties of solutal concentration profiles are seen in Figure 6. Figure 7 and Figure 8 show the behavior of various values of the Hartman number on the velocity and temperature profiles when the other physical parameters are fixed. Figure 7 shows that the dimensionless radial

Preprints (www.preprints.org) | NOT PEER-REVIEWED | Posted: 17 March 2017 doi:10.20944/preprints201703.0138.v1

Peer-reviewed version available at Entropy 2017, 19, 168; doi:10.3390/e19070168

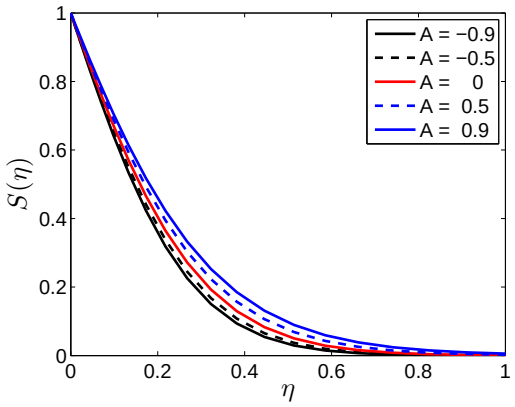

Figure 6. Effect of the unsteadiness parameter (A) on concentration profile $S(\eta)$ when $n = 3, Ha = 0.5, Nr = 0.2, Pr = 7, Nb = 0.5, Nt = 0.5, Nd = 0.02, Sc = 7, R_0 = 0.3, Ld = 0.02, \beta_i = 0.2$.

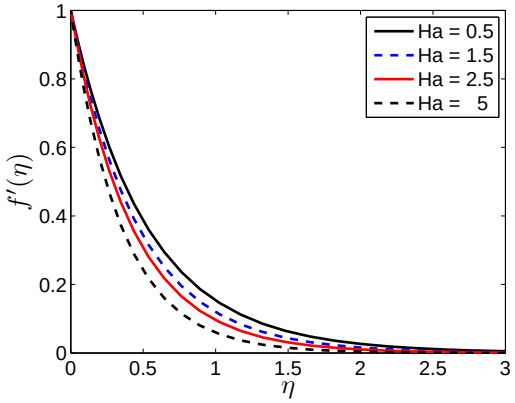

Figure 7. Effect of the Hartman number (Ha) on velocity profile $f'(\eta)$ for $n = 3, A = 0.3, Nr = 0.2, Pr = 7, Nb = 0.5, Nt = 0.5, Nd = 0.02, Sc = 7, R_0 = 0.3, Ld = 0.02, \beta_i = 0.2$.

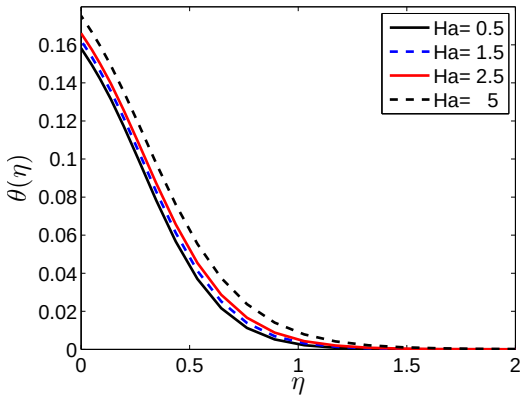

Figure 8. Effect of the Hartman number (Ha) on temperature profile $\theta(\eta)$ when $n = 3, A = 0.3, Nr = 0.2, Pr = 7, Nb = 0.5, Nt = 0.5, Nd = 0.02, Sc = 7, R_0 = 0.3, Ld = 0.02, \beta_i = 0.2$.

component of the velocity decreases as the Hartman number increases. This indicates that the Lorentz force slows the motion of the fluid in the radial direction; consequently, the boundary layer thickness increases as well. As a result velocity profile decreases as the Hartman number increase. Hence, the magnetic field can be used to control the momentum boundary layer thickness. Figure 8 provides that

Preprints (www.preprints.org) | NOT PEER-REVIEWED | Posted: 17 March 2017 doi:10.20944/preprints201703.0138.v1

Peer-reviewed version available at Entropy 2017, 19, 168; doi:10.3390/e19070168

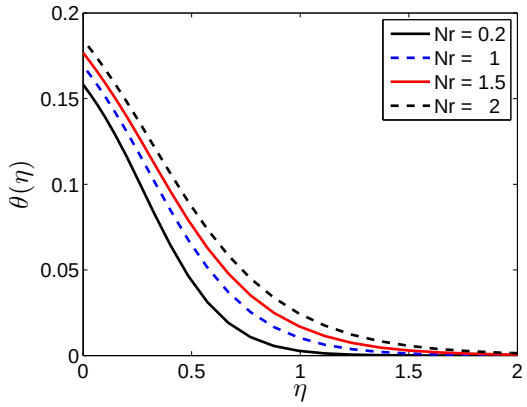

Figure 9. Effect of the thermal radiation parameter (Nr) on temperature profile $\theta(\eta)$ where $n = 3, A = 0.3, Ha = 0.5, Pr = 7, Nb = 0.5, Nt = 0.5, Nd = 0.02, Sc = 7, R_0 = 0.3, Ld = 0.02, \beta_i = 0.2$.

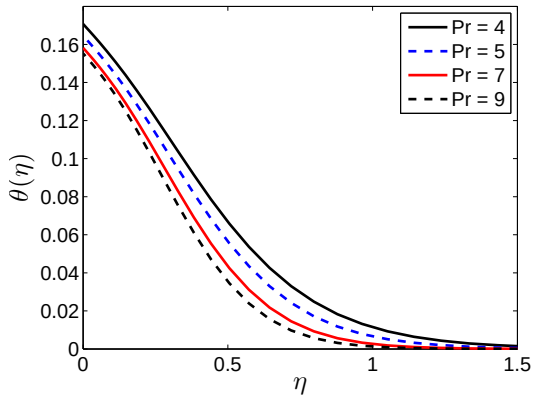

Figure 10. Effect of the Prandtl number (Pr) on temperature profile $\theta(\eta)$ for $n = 3, A = 0.3, Ha = 0.5, Nr = 0.2, Nb = 0.5, Nt = 0.5, Nd = 0.02, Sc = 7, R_0 = 0.3, Ld = 0.02, \beta_i = 0.2$.

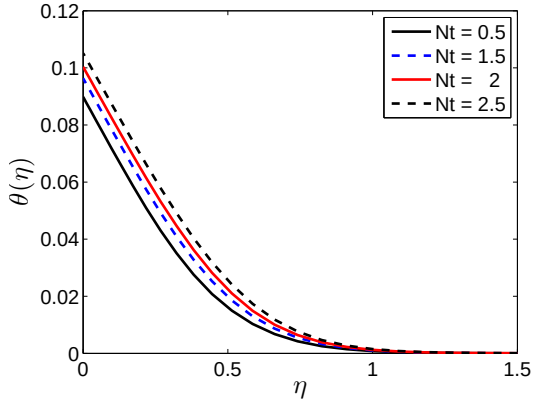

Figure 11. Effect of the thermophoresis parameter (Nt) on the temperature profile $\theta(\eta)$ for $n = 3, A = 0.3, Ha = 0.5, Nr = 0.2, Pr = 7, Nb = 0.5, Nd = 0.02, Sc = 7, R_0 = 0.3, Ld = 0.02, \beta_i = 0.2$.

the temperature profile increases with increase in the value of the Hartman number due to the effect of transverse magnetic field in the fluid. It is also worth noting that the application of the magnetic field affects the thermal boundary layer thickness positively since the thickness of the thermal boundary increases in the presence of the magnetic field. Figure 9 shows the variation of the temperature

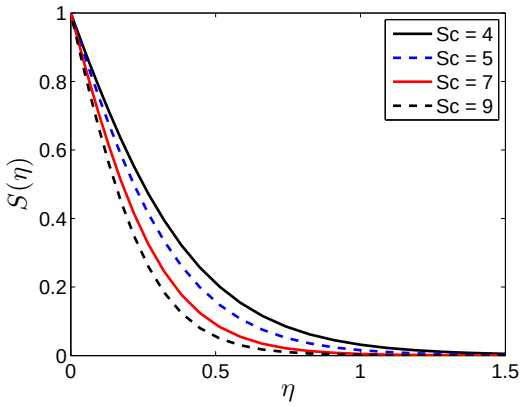

Figure 12. Effect of the Schmidt number (Sc) on concentration profile $S(\eta)$ for $n = 3, A = 0.3, Ha = 0.5, Nr = 0.2, Pr = 7, Nb = 0.5, Nt = 0.5, R_0 = 0.3, \beta_i = 0.2$.

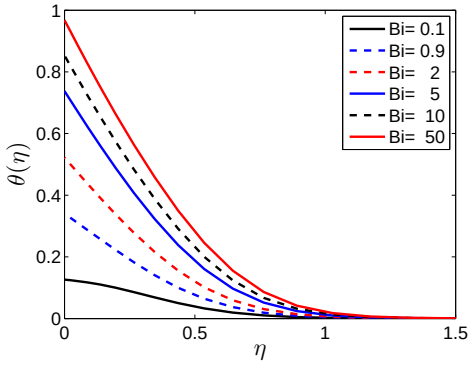

Figure 13. Effect of the Biot number (Bi) on temperature profile $\theta(\eta)$ for $n = 3, A = 0.3, Ha = 0.5, Nr = 0.2, Pr = 7, Nb = 0.5, Nt = 0.5, Nd = 0.02, Sc = 7, R_0 = 0.3, Ld = 0.02$.

profiles for different values of the thermal radiation parameter. The temperature profiles increases with increased thermal radiation which is in line with physical observations regarding the impact of increasing thermal radiation.

Figure 10 presents the influence of the Prandtl number on the temperature profile by fixing values of other parameters. It is clear that as the Prandtl number increases, the temperature profiles decrease. Smaller Prandtl numbers suggest a fluid with higher thermal conductivities hence heat diffuses more rapidly from the heated surface than in the case of fluids with higher Prandtl numbers. Figure 11 illustrates the variation of the temperature profiles with different values of the thermophoresis parameter, Nt when the other parameter are fixed. It is observed the temperature profile increases as the thermophoresis parameter increases because the thermal boundary layer increases with increases in the thermophoresis parameter.

Figure 12 illustrates the influence of Schmidt number on the solutal concentration profile with fixing the other parameters. It it clear that the solutal concentration profile decreases as the Schmidt number increases.

Figure 13 depicts the influence of the Biot number Bi on the temperature profiles. The Biot number can be perceived as the ratio of internal (conductive) resistance of solid to external (convective resistance). Here we observe that an increase in the Biot number leads to enhanced temperature profiles. An increase in the Biot number causes a stronger convection and this leads to higher surface temperatures. Further, for sufficiently large values of the Biot number, the temperature profile approaches its maximum value. Figure 14 shows that an increase in the power-law index leads

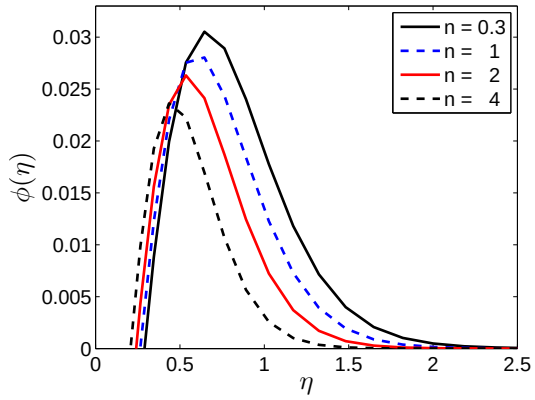

Figure 14. Effect of the stretching parameter (n) on the nanofluid volume fraction profile $\phi(\eta)$ when $A = 0.3, Ha = 0.5, Nr = 0.2, Pr = 7, Nb = 0.5, Nt = 0.5, Nd = 0.02, Sc = 7, R_0 = 0.3, Ld = 0.02, \beta_i = 0.2$.

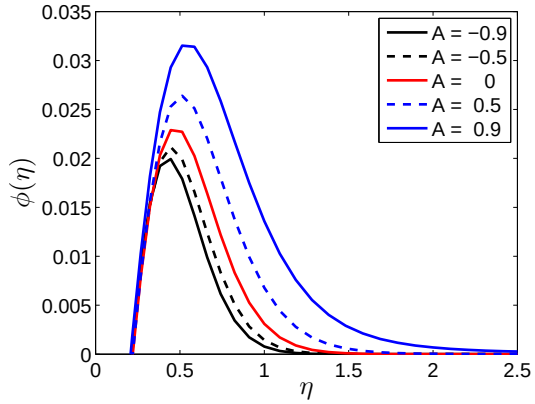

Figure 15. Effect of the unsteadiness parameter (A) on nanofluid volume fraction profile $\phi(\eta)$ for $n = 3, Ha = 0.5, Nr = 0.2, Pr = 7, Nb = 0.5, Nt = 0.5, Nd = 0.02, Sc = 7, R_0 = 0.3, Ld = 0.02, \beta_i = 0.2$.

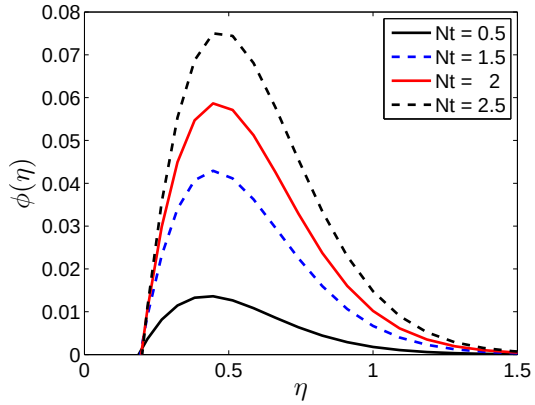

Figure 16. Effect of the thermophoresis parameter (Nt) on the nanofluid volume fraction profile $\phi(\eta)$ for $n = 3, A = 0.3, Ha = 0.5, Nr = 0.2, Pr = 7, Nb = 0.5, Nd = 0.02, Sc = 7, R_0 = 0.3, Ld = 0.02, \beta_i = 0.2$.

to a reduction in the thickness of the nanoparticle concentration boundary layer thickness up to a certain value of η. Beyond this critical distance, the opposite trend is observed. In Figure 15, we

Preprints (www.preprints.org) | NOT PEER-REVIEWED | Posted: 17 March 2017 doi:10.20944/preprints201703.0138.v1

Peer-reviewed version available at Entropy 2017, 19, 168; doi:10.3390/e19070168

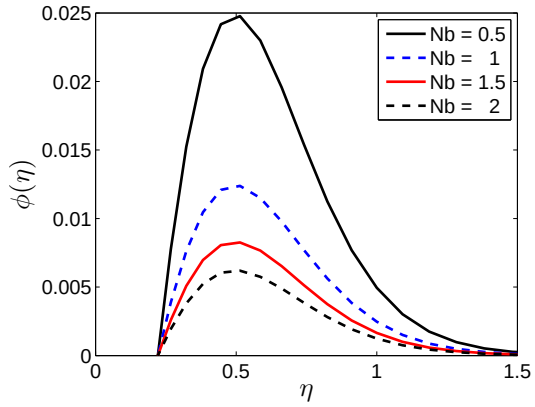

Figure 17. Effect of the Brownian motion parameter (Nb) on nanofluid volume fraction profile $\phi(\eta)$ when $n = 3, A = 0.3, Ha = 0.5, Nr = 0.2, Pr = 7, Nt = 0.5, Nd = 0.02, Sc = 7, R_0 = 0.3, Ld = 0.02, \beta_i = 0.2$.

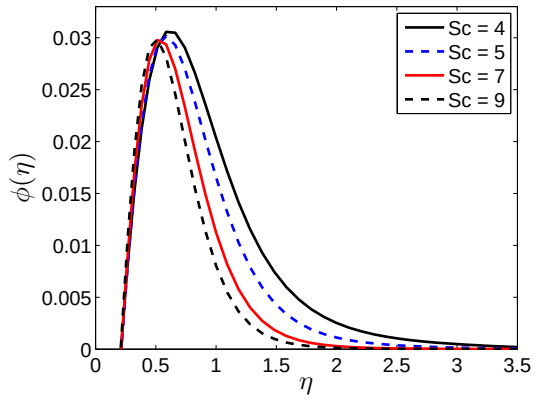

Figure 18. Effect of the Schmidt number (Sc) on nanofluid volume fraction profile $\phi(\eta)$ for $n = 3, A = 0.3, Ha = 0.5, Nr = 0.2, Pr = 7, Nb = 0.5, Nt = 0.5, R_0 = 0.3, \beta_i = 0.2$.

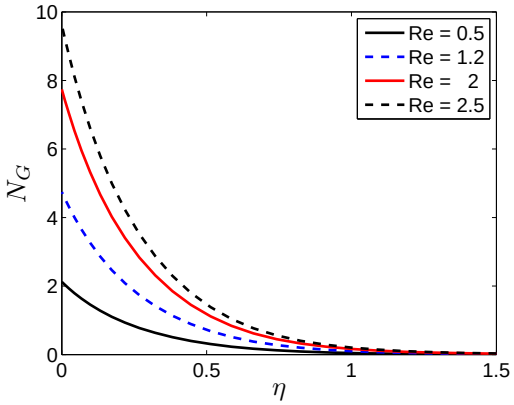

Figure 19. Effect of the Reynolds number Re on the entropy generation number N_G when $Nr = 0.2, Br = 1, \Omega = 1, Ha = 0.5$ and $\Sigma = 0.5$.

note a similar pattern of nanoparticle concentration profiles as in Figures 5 and 6. In Figure 16 we note that the nanoparticle concentration profiles increase with the thermophoresis parameter. Similar results are shown in Figure 17 for the Brownian motion parameter. In Figure 18, it is observed that

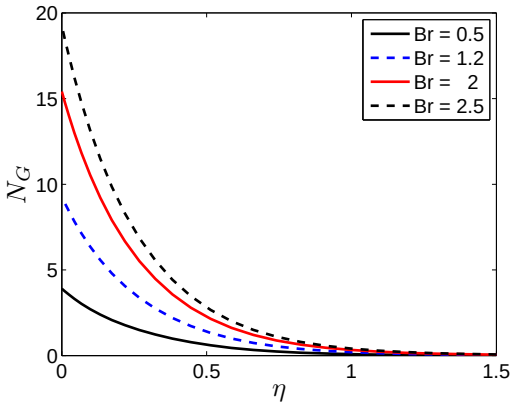

Figure 20. Effect of Brinkman number Br on the entropy generation number N_G when $Re = 2, Nr = 0.2, \Omega = 1, Ha = 0.5$ and $\Sigma = 0.5$.

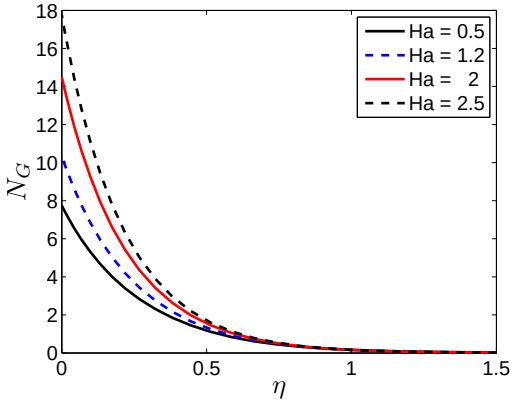

Figure 21. Effect of Hartman number Ha on the entropy generation number N_G when $Re = 2, Nr = 0.2, Br = 1, \Omega = 1$ and $\Sigma = 0.5$.

increasing the Schmidt number reduces the nanoparticle concentration profile. The impact of the Schmidt number Sc is inversely proportional to that of the Brownian diffusion coefficient. When D_B is small the penetration depth of the nanoparticle concentration profiles becomes shorter. Thus, as the Schmidt number increases the penetration depth becomes shorter. Moreover the increase in Sc leads to decrease in both the concentration rate and the heat transfer rate.

It is interesting to note that Figures 19 - 23 suggest different ways of controlling the entropy generation number. Figure 19 shows the effect of the Reynolds number on the entropy generation N_G. It is observed that an increase in the Reynolds number leads to an increase in the entropy generation number. This may be attributed to the fact that an increase in Re corresponds to an increase in random eddies, vortices and flow fluctuation in the fluid which in turn increases the heat transfer rate. An increase in heat transfer leads to an increase in the randomness of the system thereby leading to an increase in N_G. The entropy generation number increases in the proximity of the sheet due to a decrease in the fluid friction. Reducing the Reynolds number induces a reduction in the entropy generation number.

Figure 20 shows the behavior of entropy generation number with varying values of Brinkman number. The Brinkman number is a measure of the importance of heat produced by viscous dissipation (viscous heating) relative to heat transported by molecular conduction (conductive heat transfer). Increasing the Brinkman number causes an increase in the entropy generation number in the vicinity of the sheet. Heat produced by viscous dissipation dominates over heat transported

Preprints (www.preprints.org) | NOT PEER-REVIEWED | Posted: 17 March 2017 doi:10.20944/preprints201703.0138.v1

Peer-reviewed version available at Entropy 2017, 19, 168; doi:10.3390/e19070168

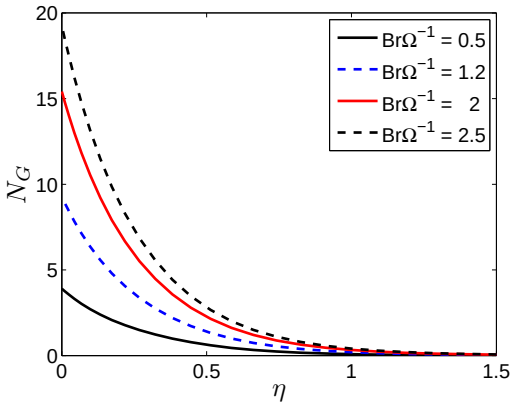

Figure 22. Effect of the Brinkman group parameter $Br\Omega^{-1}$ on the entropy generation number N_G when $Re = 2, Nr = 0.2, Br = 1$ and $\Sigma = 0.5$.

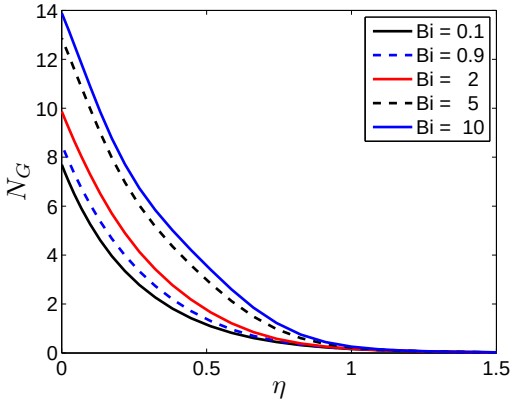

Figure 23. Effect of Biot number Bi on the entropy generation number N_G when $Re = 2, Nr = 0.2, Br = 1, Ha = 0.5, \Omega = 1$ and $\Sigma = 0.5$.

by molecular conduction in the proximity of the sheet. In the vicinity of the sheet, significant heat generation occurs within the layers of the moving fluid particles which in turn increases the entropy generation number by enhancing the degree of disorder of the system. This effect gradually fades out with the distance from the sheet.

The influence of the Hartman number on the entropy generation number is depicted in Figure 21. In close proximity to the sheet, an increase in the Hartman number corresponds to a noticeable increase in the entropy generation number whereas far from the sheet the increase in the Hartman number has rather negligible effect on the entropy generation number. This observed behavior of the entropy generation number in response to the Hartman number is related to the increase in the resistance of the fluid motion due to the increasing Hartman number and that causes higher heat transfer rate which results in an increase on the entropy generation number. However, at far away distance from the sheet the effect of Hartman number is insignificant causing the corresponding insignificant entropy generation number.

Figure 22 displays the entropy generation number with changing values of the Brinkman group of parameter ($Br\Omega^{-1}$). The increase in $Br\Omega^{-1}$ has a remarkable effect on the entropy generation number in the proximity of the sheet. The increase in the entropy generation number around the sheet due to the increase in $Br\Omega^{-1}$ can be related to a decrease in the fluid friction caused by increasing $Br\Omega^{-1}$. Moreover, Equation (31) suggests that the increase in $Br\Omega^{-1}$ results in increase in the sheet velocity which affects the fluid in the surroundings of the sheet and that explains, in part,

the noticeable effect of $Br\Omega^{-1}$ on the entropy generation proximity of the sheet and the negligible effect in the further region. Figure 23 demonstrates the relation between the Biot number and the entropy generation number. With increasing Biot number the entropy generation number increases prominently in the proximity of the sheet whereas the effect of the Biot number on the entropy generation number is insignificant in the region far away from the sheet.

6. Conclusion

We have presented a mathematical formulation and analysis for the entropy generation rate in an unsteady three dimensional axisymmetric MHD nanofluid flow over a non-linear stretching sheet with thermal radiation and a chemical reaction. The importance of different physical parameters on the entropy generation number are has been demonstrated and discussed in detail. From the discussion, the following outcomes may be inferred;

1. The heat transfer rate increases with increasing sheet stretching.
2. An increase in the Reynolds number and the Brinkman number corresponds to a significant increase in the entropy generation number. Therefore, it can be ascertained that viscous dissipation effect on entropy generation is significant for a nanofluid flow with a high Reynolds number.
3. An increase in the Biot and Hartman numbers corresponds to significant increase in entropy generation number in the vicinity of the sheet surface. The significance of the Biot and Hartman numbers gradually fades with distance from the sheet.
4. The entropy generation rate can be minimized by controlling the physical parameters.

Acknowledgments: The authors would like to thank the University of KwaZulu-Natal and Claude Leon Foundation, South Africa for the financial support.

Author Contributions: Mondal proposed the main idea and design the framework. Almakki carried out the numerical part and done first write-up of this paper. Dey revised the write-up and did analyses in some section of the write-up. Finally, Sibanda checked the whole write-up and numerical calculation. All authors contribute equally in the analysis of the results.

Bibliography

1. Dessie, H.; Kishan, N. Unsteady MHD flow of heat and mass transfer of nanofluids over stretching sheet with a non-uniform heat/source/sink considering viscous dissipation and chemical reaction. International Journal of Engineering Research in Africa. Trans Tech Publ, 2015, Vol. 14, pp. 1–12.
2. Chol, S. Enhancing thermal conductivity of fluids with nanoparticles. *ASME-Publications-Fed* **1995**, *231*, 99–106.
3. Buongiorno, J. Convective transport in nanofluids. *Journal of Heat Transfer* **2006**, *128*, 240–250.
4. Ahmed, N.; Goswami, J.; Barua, D. Effects of chemical reaction and radiation on an unsteady MHD flow past an accelerated infinite vertical plate with variable temperature and mass transfer. *Indian Journal of Pure and Applied Mathematics* **2013**, *44*, 443–466.
5. Ahmed, J.; Mahmood, T.; Iqbal, Z.; Shahzad, A.; Ali, R. Axisymmetric flow and heat transfer over an unsteady stretching sheet in power law fluid. *Journal of Molecular Liquids* **2016**, *221*, 386–393.
6. Mohammadiun, H.; Rahimi, A.; Kianifar, A. Axisymmetric stagnation-point flow and heat transfer of a viscous, compressible fluid on a cylinder with constant heat flux. *Scientia Iranica* **2013**, *20*, 185–194.
7. Shankar, B.; Yirga, Y. Unsteady heat and mass transfer in MHD flow of nanofluids over stretching sheet with a non-uniform heat source/sink. *International Journal of Mathematical, Computational Science and Engineering* **2013**, *7*, 1267–1275.
8. Shahzad, A.; Ali, R.; Khan, M. On the exact solution for axisymmetric flow and heat transfer over a nonlinear radially stretching sheet. *Chinese Physics Letters* **2012**, *29*, 084705.
9. Ahmad, S.; Ashraf, M.; Syed, K. Effects of thermal radiation on MHD axisymmetric stagnation point flow and heat transfer of a micropolar fluid over a shrinking sheet. *World Applications Science Journal* **2011**, *15*, 835–848.

10. Mabood, F.; Shafiq, A.; Hayat, T.; Abelman, S. Radiation effects on stagnation point flow with melting heat transfer and second order slip. *Results in Physics* **2017**, *7*, 31–42.
11. Prasad, K.; Vaidya, H.; Vajravelu, K.; Datti, P.; Umesh, V. Axisymmetric mixed convective MHD flow over a slender cylinder in the presence of chemically reaction. *International Journal of Applied Mechanics and Engineering* **2016**, *21*, 121–141.
12. Sarada, K.; Shanker, B. The effect of chemical reaction on an unsteady MHD free convection flow past an infinite vertical porous plate with variable suction. *International Journal of Engineering Modern Research* **2013**, *3*, 725–735.
13. Hunegnaw, A.; Kishan, N. Unsteady MHD heat and mass transfer flow over stretching sheet in porous medium with variable properties considering viscous dissipation and chemical reaction. *Am. Chem. Sci. J* **2014**, *4*, 901–917.
14. Barik, R. Heat and Mass Transfer Effects on Unsteady MHD Flow through an Accelerated Isothermal Vertical Plate Embedded in Porous Medium in the Presence of Heat Source and Chemical Reaction. *European Journal of Advances in Engineering and Technology* **2016**, *3*, 56–61.
15. Bejan, A. *Entropy generation minimization: the method of thermodynamic optimization of finite-size systems and finite-time processes*; CRC press, 1995.
16. Qing, J.; Bhatti, M.M.; Abbas, M.A.; Rashidi, M.M.; Ali, M.E.S. Entropy generation on MHD Casson nanofluid flow over a porous stretching/shrinking surface. *Entropy* **2016**, *18*, 123.
17. Rashidi, M.; Mohammadi, F.; Abbasbandy, S.; Alhuthali, M. Entropy generation analysis for stagnation point flow in a porous medium over a permeable stretching surface. *J Appl Fluid Mech* **2015**, *8*, 753–765.
18. Rashidi, M.; Abelman, S.; Mehr, N.F. Entropy generation in steady MHD flow due to a rotating porous disk in a nanofluid. *International Journal of Heat and Mass Transfer* **2013**, *62*, 515–525.
19. Freidoonimehr, N.; Rahimi, A.B. Comment on "Effects of thermophoresis and Brownian motion on nanofluid heat transfer and entropy generation" by M. Mahmoodi, Sh. Kandelousi, Journal of Molecular Liquids, 211 (2015) 15–24. *Journal of Molecular Liquids* **2016**, *216*, 99–102.
20. Agbaje, T.; Mondal, S.; Makukula, Z.; Motsa, S.; Sibanda, P. A new numerical approach to MHD stagnation point flow and heat transfer towards a stretching sheet. *Ain Shams Engineering Journal* **2016**.
21. Kaladhar, K.; Motsa, S.; Srinivasacharya, D. Mixed Convection Flow of Couple Stress Fluid in a Vertical Channel with Radiation and Soret Effects. *Journal of Applied Fluid Mechanics* **2016**, *9*, 43–50.
22. Nield, D.; Kuznetsov, A. The onset of convection in a horizontal nanofluid layer of finite depth: A revised model. *International Journal of Heat and Mass Transfer* **2014**, *77*, 915–918.
23. Mustafa, M.; Khan, J.A.; Hayat, T.; Alsaedi, A. Analytical and numerical solutions for axisymmetric flow of nanofluid due to non-linearly stretching sheet. *International Journal of Non-Linear Mechanics* **2015**, *71*, 22–29.
24. Sajid, M.; Hayat, T.; Asghar, S.; Vajravelu, K. Analytic solution for axisymmetric flow over a nonlinearly stretching sheet. *Archive of Applied Mechanics* **2008**, *78*, 127–134.
25. Pal, D. Heat and mass transfer in stagnation-point flow towards a stretching surface in the presence of buoyancy force and thermal radiation. *Meccanica* **2009**, *44*, 145–158.
26. Arikoglu, A.; Ozkol, I.; Komurgoz, G. Effect of slip on entropy generation in a single rotating disk in MHD flow. *Applied Energy* **2008**, *85*, 1225–1236.
27. Bellman, R.E.; Kalaba, R.E. Quasilinearization and nonlinear boundary-value problems, 1965.
28. Canuto, C.; Hussaini, M.Y.; Quarteroni, A.M.; Thomas Jr, A.; others. *Spectral methods in fluid dynamics*; Springer Science & Business Media, 2012.
29. Trefethen, L.N. *Spectral methods in MATLAB*; SIAM, 2000.
30. Motsa, S.; Sibanda, P.; Shateyi, S. On a new quasi-linearization method for systems of nonlinear boundary value problems. *Mathematical Methods in the Applied Sciences* **2011**, *34*, 1406–1413.